Biochemical and Biophysical Research Communications 458 (2015) 40–45

Contents lists available at ScienceDirect

Biochemical and Biophysical Research Communications

journal homepage: www.elsevier.com/locate/ybbrc

Optical imaging of COX-2: Studies on an autofluorescent 2,3-diaryl-substituted indole-based cyclooxygenase-2 inhibitor

Christoph Tondera [a, b], Sandra Ullm [a, b], Markus Laube [a, b], Sebastian Meister [a], Christin Neuber [a], Birgit Mosch [a], Torsten Kniess [a], Jens Pietzsch [a, b, *]

[a] Helmholtz-Zentrum Dresden-Rossendorf, Institute of Radiopharmaceutical Cancer Research, Department of Radiopharmaceutical and Chemical Biology, Dresden, Germany
[b] Technische Universität Dresden, Department of Chemistry and Food Chemistry, Dresden, Germany

ARTICLE INFO

Article history:
Received 10 January 2015
Available online 27 January 2015

Keywords:
Fluorescence
Luminescence
Phorbol myristate ester-induced COX-2 expression
Melanoma-associated inflammation
Rodent melanoma xenograft model

ABSTRACT

This study aimed at *in vivo* visualization of cyclooxygenase-2 (COX-2) by optical imaging using a representative compound of a class of autofluorescent 2,3-diaryl-substituted indole-based selective COX-2 inhibitors (2,3-diaryl-indole coxibs). COX-2 was successfully visualized in mice models with phorbol myristate ester (TPA)-induced inflammation or bearing xenografted human melanoma cells by 2-[4-(aminosulfonyl)phenyl]-3-(4-methoxyphenyl)-1*H*-indole (**C1**). COX-2 protein expression in both TPA-induced inflammatory sites and human melanoma xenografts was confirmed by immunoblotting. Control experiments using surrogate markers, sham injections, and non-COX-2 expressing melanoma cells further confirmed specificity of tissue association of **C1**. The merging of therapeutic and diagnostic properties of 2,3-diaryl-indole coxibs may widen the range of applications of COX-2-targeted treatment, e.g., for *in situ*-guided surgery and *ex vivo* diagnostics.

1. Introduction

Cyclooxygenase-2 (COX-2) is the inducible isoenzyme of cyclooxygenases (prostaglandin-H-synthases, EC 1.14.99.1) whose overexpression is implicated in a number of inflammatory or inflammation-associated processes [1]. COX-2 is mostly induced as reaction to inflammatory and proliferative stimuli [2], e.g. hypoxia [3–6], glucose deprivation [7] or chemicals such as 12-*O*-tetradecanoylphorbol-13-acetat (TPA) [8,9]. Due to the structural similarity of TPA to diacyglycerol, TPA directly activates protein kinase C. Protein kinase C in turn activates NFκB, which transcriptionally induces COX-2 gene expression [10,11]. Interestingly, a high COX-2 expression and activity is also found in many tumor entities including the majority of human epithelium-derived malignant tumors. Hence, COX-2 expression is implicated in tumor inflammogenesis, proliferation, angiogenesis, metastasis and radiosensitivity of these tumors [5,12]. Human melanoma, a non-epithelial tumor, shows a distinct inflammatory response as well as a metastatic behavior. In addition, most of these tumors express COX-2, which appears to be involved in the regulation of melanoma invasion [13]. Consequently, blocking the COX-2 isoenzyme selectively provides a number of therapeutic strategies such as the inhibition of the progression of COX-2 expressing tumors or the increase of their susceptibility to radiotherapy [14,15]. The specificity of COX-2 expression is suggesting the use of selective COX-2 inhibitors for the diagnosis of inflammatory lesions and COX-2 expressing tumor entities by means of imaging technologies whereby unspecific enrichment in other organs may be avoided. To this end, we developed a series of novel potential coxibs based on a 2,3-diaryl-substituted indole lead structure with high affinity and selectivity for COX-2 as appropriate templates for radiotracer design [16]. For our efforts the high potential of both varying the C-2/C-3 substitution pattern in the indole scaffold, e.g., by introducing fluorine or methoxy groups, and using a highly effective synthesis route via McMurry cyclization was of particular interest [5,16]. The indole motif, on the other hand, is also a prominent

Abbreviations: COX-2, cyclooxygenase-2; DMSO, dimethyl sulfoxide; FWHM, full width at half maximum; TPA, 12-*O*-Tetradecanoylphorbol-13-acetat; i.p., intraperitoneal; EPR, enhanced permeability and retention.

* Corresponding author. Helmholtz-Zentrum Dresden-Rossendorf, Institute of Radiopharmaceutical Cancer Research, Department of Radiopharmaceutical and Chemical Biology, Dresden, Germany.
E-mail address: j.pietzsch@hzdr.de (J. Pietzsch).

http://dx.doi.org/10.1016/j.bbrc.2015.01.057
0006-291X/

fluorophore [17,18]. Thus, these 2,3-diaryl-substituted indole-based cyclooxygenase-2 inhibitors (2,3-diaryl-indole coxibs) exhibited physicochemical properties such as strong autofluorescent activity [16], therefore suggesting to be promising compounds for novel fluorescence based imaging of COX-2. On the other hand, COX-2 inhibitors with covalently coupled fluorophores already have been developed and characterized as specific fluorescent imaging agents of COX-2 expression *in vitro* and *in vivo* [19–21]. In a preliminary investigation the 2,3-diaryl-indole coxib, 2-[4-(aminosulfonyl)phenyl]-3-(4-methoxyphenyl)-1*H*-indole (**C1**; IC_{50}(COX-2) = 0.006 nM, IC_{50}(COX-2) > 10 μM) [22], has been demonstrated to be a powerful imaging agent for the characterization of specific subcellular binding of coxibs to their target enzyme using confocal cryofluorescence microscopy in melanoma cell culture *in vitro* [23]. As a great benefit, measurements at cryogenic temperatures (20 K) show much higher quantum yields and, therefore, allow for the use of very low concentrations (0.1 nM) of the inhibitor [23]. However, we assumed that the use of higher, pharmacologically relevant concentrations of this autofluorescent coxib would also allow *in vivo* and *ex vivo* visualization of COX-2 in tissues at room temperature. This approach could provide further information on pharmacological properties of this selected coxib as a representative compound of a whole class of indole-based coxibs without the need of further modification by radio- or fluorescent labeling. This encouraged us to undertake a detailed *in vivo* and *ex vivo* investigation to further characterize *i*) specific targeting of COX-2 in inflammatory and tumor lesions using the compound **C1** and *ii)* its overall biodistribution and elimination in rodent models.

2. Materials and methods

2.1. Chemical synthesis and fluorescence properties

The selective COX-2 inhibitor 2-[4-(aminosulfonyl)phenyl]-3-(4-methoxyphenyl)-1*H*-indole (**C1**) was synthesized as published elsewhere, the analysis of the fluorescence properties of **C1** was previously published by our group [16,22,23]. The compound showed a bright fluorescence at an excitation of 345 nm and an emission of 482 nm.

2.2. Animal experiments

All animal procedures and experiments were carried out according to guidelines of the German Regulations for Animal Welfare. The protocols were approved by the local Ethical Committee for Animal Experiments. In order to characterize a non-tumor associated COX-2 expression female immunocompetent NMRI mice (30–35 g, n = 3) were used. COX-2 expression was chemically induced by injecting 200 μL TPA (100 μM) in the right armpit and 100 μL TPA behind the right ear on the first day of the experiment. Consecutively, at the second and third day high COX-2 expression was maintained with injections of 20 μL TPA in the armpit and 10 μL behind the ear. The same procedure was done with isotonic injection solution (E153) on the left side (sham) of the mice. As an independent surrogate control measurement to prove successful induction of the proinflammatory process the luminol derivative L-012 (Wako Chemicals, Virginia, USA) was used, which reacts with reactive oxygen species, e.g., formed by NADPH oxidase, leading to the emission of photons [24–26]. Therefore, mice were anesthetized with desfluran (9–10% v/v, 30% oxygen air) and put in supine position. 500 μg L-012 were injected intraperitoneally (i.p.) in each mouse in 100 μL isotonic sodium chloride. The luminescence was measured using the dedicated small-animal In-vivo Imaging System FX Pro (Carestream Health, USA) in luminescence mode (no filter) with an exposure time of 10 min and a 4 × 4 binning. The pictures were merged with the X-ray acquisitions. In order to characterize melanoma-associated COX-2 expression athymic nude NMRI mice bearing human melanoma xenografts were used. The human malignant melanoma cell lines A2058, A375-pIRES and A375-EphB4 were cultivated as described elsewhere in detail [27]. Of note, the transgenic A375 cell lines (A375-pIRES and A375-EphB4) were developed in context of another investigation published by us elsewhere [28]. Subcutaneous xenograft tumor models of A375 and A2058 cell lines were generated by injecting 5 × 10^6 cells (passages 5–10) in 100 μL isotonic sodium chloride in the right thigh (A2058) or both thighs (A375-pIRES, left side and A375-EphB4, right side) of female nude NMRI mice (30–35 g, n = 9; A2058 xenografts (n = 5); A375 xenografts (n = 4)) as described elsewhere in detail [28]. The tumors were grown over 2–3 weeks to a maximum size of 1 cm^3. For COX-2 imaging experiments a 20 mM injection solution of **C1** was prepared in DMSO. The mice were anesthetized with desfluran (9–10% v/v, 30% oxygen air). Animals were put in supine position and injected intraperitoneally with 100 μL of the injection solution. Fluorescence measurements were conducted using the In-vivo Imaging System FX Pro (Carestream Health, USA) with an exposure time of 15 min and a 4 × 4 binning. An excitation filter for 340 nm (FWHM 10 nm, Edmund Optics, Barrington, USA) and an emission filter for 480 nm (FWHM 110 nm, Carestream Health, USA) were used. The fluorescence pictures were merged with the conducted X-ray acquisition using Carestream Molecular Imaging software. After the measurements the animals were sacrificed and 80 μm thick whole animal coronal cryosections were prepared using a Leica Jung Cryopolycut (Leica Microsystems, Wetzlar, Germany). The cryosections were put on foils and lyophilized. Subsequently, the sections were measured in the In-vivo Imaging System FX Pro and scanned. For a better resolution the exposure time was set to 30 min and no binning was performed. For the sections same filter settings were used as described for the whole animal acquisition.

2.3. Determination of COX-2 expression

In order to detect COX-1 and COX-2 expression in the used cells and animal tissues Western blotting was performed. Therefore cells were lyzed as described previously [27]. Tissue samples from the TPA-injected mice (inflammatory site and sham tissue at 3rd day post injection) and tumors from xenograft models were explanted out of the euthanized animals, homogenized in the TissueLyser (Qiagen Germany) in RIPA lysis buffer (150 mM NaCl, 50 mM Tris pH 8.0, 1% NP40, 0.5 wt.-% SDS, 7 μg/mL leupeptin, 1 mM PMSF, 1 mM Na_3VO_4, 1 mM DTT, 7 mM NaF) three cycles for each 3 min with a frequency of 25 Hz. SDS-PAGE and Western blotting were performed as described previously [27,29].

3. Results

3.1. Determination of COX-2 expression

The Western blot analysis of cells, xenograft and inflammation tissue lysates is shown in Fig. 1. A2058 cells and the corresponding xenograft tumors show a high expression of COX-2 and a basal level of COX-1 synthesis, which is less in the tumor lysates. A375-EphB4 cells show no COX-2 expression, whereas A375-pIRES cells and the tumor lysates express very low levels of COX-2. Interestingly, in A375-pIRES derived tumors we found a higher expression of COX-1 compared to the A2058 tumors (Fig 1B). Tissue obtained from TPA-induced inflammatory lesions also exhibit high COX-2 expression (Fig. 1C). At the sham injection site no expression of either COX-1 or COX-2 could be detected.

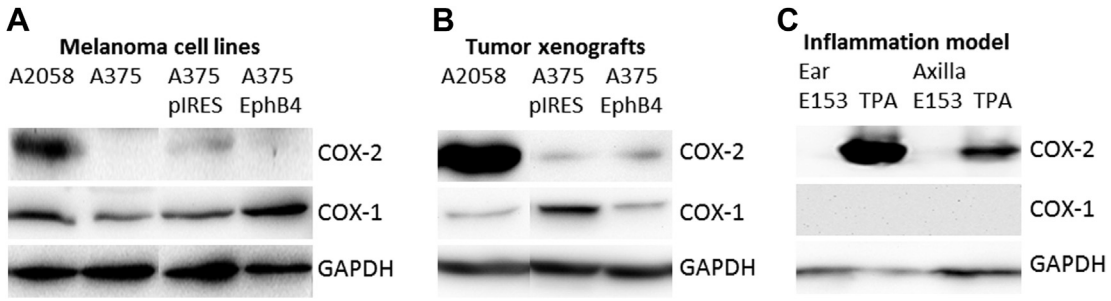

Fig. 1. Expression of COX-2 and COX-1 in (A) human melanoma cell lines A2058 and A375 (wild type, pIRES: transfection control, EphB4: transfection with EphB4), (B) tumor xenograft models of human melanoma cell lines A2058 and A375 (pIRES: transfection control, EphB4: transfection with EphB4) in nu/nu mice, and (C) in NMRI mice after chemical induction of COX-2 expression by injection of 100 μM TPA in PBS or control injection with E153 in ear and axilla region. The figure shows a representative Western blot out of 3 (cell lysates and animals) independent experiments.

3.2. COX-2 visualization

3.2.1. Non-tumor associated COX-2 expression

In Fig. 2 the non-tumor model is presented. The injection of the luminol derivative L-012 shows a strong luminescence signal in both inflammatory sites (ear and axilla) on the right side of the animal (Fig. 2A). On the left side no signal could be detected, which suggests that no production of reactive oxygen species occurred. We therefore conclude that no inflammation was induced by the injection of isotonic sodium chloride.

After intraperitoneal injection of **C1** emission of fluorescence at the inflammatory site was observed after 5 h (Fig. 2B). In contrast to the luminescence signal only a single fluorescent region was located at the ear of the mice on the right side. The signal occurred directly behind the ear where the animals have less fur. On the left side no fluorescence signal was present. Due to the short wavelengths of the excitation and emission maxima of the compound and the resulting low penetration depth it was not possible to detect signals from the inflammatory site under the armpit in supine position.

However, a specific enrichment of **C1** could be detected at the inflammatory site behind the ear but not at the sham injection site, giving first hints towards COX-2 specific binding properties of **C1** *in vivo*.

3.2.2. Tumor associated COX-2 expression

In Fig. 3 the fluorescence acquisition of the A375 tumor xenograft model is given. Fig. 3A shows the whole animal acquisition 6 h after injection of **C1**. No significant local enrichment of the fluorescent signal (only a very weak signal) could be detected at the regions at and around the tumor. The cryosections 6 h after injection shown in Fig. 3B also confirm no local enrichment of **C1** in the tumor. In contrast, accumulation of **C1** could be observed in adipose tissue in the neck region and, more abundant, in the abdominal region of the animals. Also an amount of **C1** could be observed in the upper layers of the skin of the animals.

In contrast to the A375 tumors, which were used as negative control, the whole animal acquisition of the A2058 tumor xenograft model revealed a first local enrichment of **C1** at the tumor site after 3 h (data not shown). 5 h past injection of **C1** the signal to background ratio in the tumor region in the whole animal acquisition was highest (Fig. 4a). The maximum fluorescence intensity could be observed at 24 h post injection (Fig. 4B). However, at this time point a fluorescence signal could be detected that is distributed over almost the whole animal. Notably, cryosections after 24 h, shown in Fig. 4C, clearly revealed a local enrichment of **C1** within the tumor region. Compound enrichment was observed in the gastrointestinal system suggesting hepatobiliary elimination of the compound, as well as in the skin of the mice, most probably located in the subcutaneous fat tissue, which could explain the whole body distribution of the fluorescence signal of **C1**.

4. Discussion

This pilot study demonstrates the visualization of COX-2 in TPA-induced inflammatory lesions in NMRI mice and in human melanoma xenografts in nu/nu NMRI mice *in vivo* and *ex vivo* (in cryosections) by the use of an autofluorescent 2,3-diaryl-indole coxib. The TPA-injected mouse model could successfully be used as proof of non-tumor associated COX-2 synthesis by using the presented autofluorescent indole-based compound **C1**. However, short compound-dependent excitation wavelengths used in this study can only penetrate less than one mm deep into the tissue, hence limiting the possible detection depth [30,31]. Additionally, the fur of the NMRI mice disrupts the fluorescence signal, hindering the complete detection of the fluorescence signal in this animal model. But even though only the inflammatory site at the ear could be detected in the supine position of the animals the observed data are consistent with the literature reporting elevated COX-2 expression after TPA-injection [2]. A very weak signal around the tumor region could also be detected during whole animal acquisition in the COX-2 negative A375 tumor bearing animals. Reasons for this could be

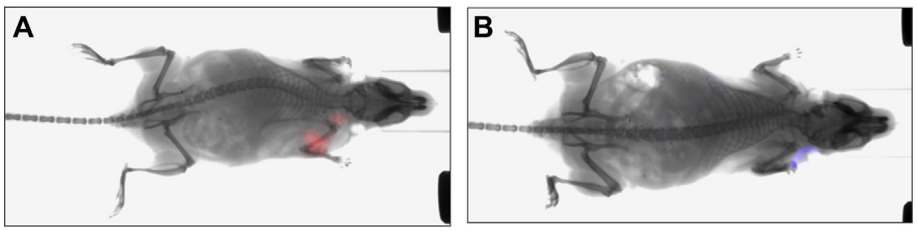

Fig. 2. Inflammation model Measurement of (A) the ROS sensitive dye L-012 direct after injection, exposure time 10 min, binning 4 × 4 and (B) C1 5 h after i.p. injection exposure time 15 min, binning 4 × 4. The figure shows representative images out of 3 independent experiments.

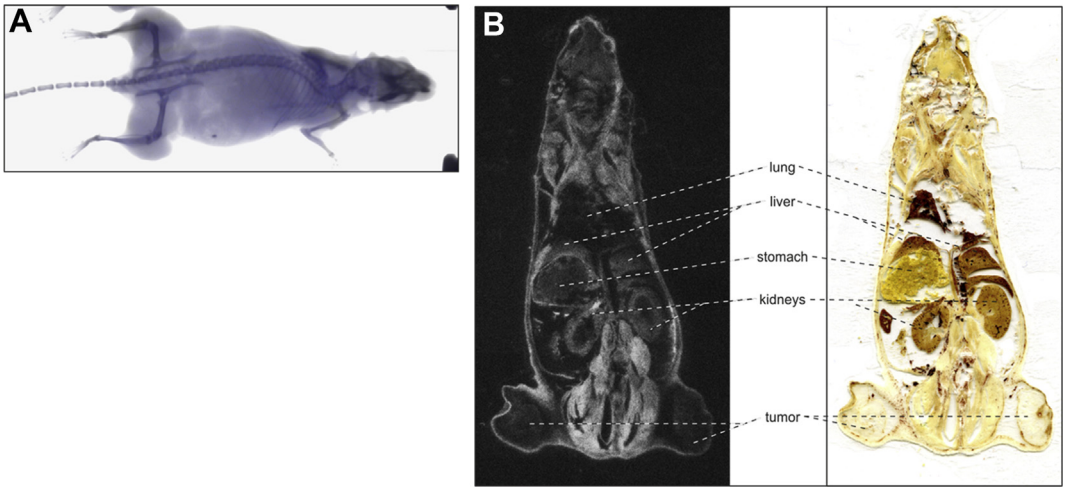

Fig. 3. A375 tumor xenograft model (A) Whole animal acquisition of A375 (A375-pIRES, left side and A375-EphB4, right side) tumor bearing mice 6 h after i.p. injection of 100 μL 20 mM **C1** exposure time 15 min, binning 4 × 4; (B) cryosection 6 h after i.p. injection of **C1**, exposure time 30 min. The figure shows representative images out of 4 independent experiments.

unspecific enrichment in subcutaneous adipose tissue or inflammatory or necrotic regions around the tumor inducing COX-2 expression [32]. This also explains the higher level of COX-2 expression in the A375 tumor xenograft models compared to levels of the different cell lines identified via immunoblotting analysis. Furthermore, the enhanced permeability and retention (EPR)-effect possibly causes increased accumulation of the low-molecular-weight, lipophilic inhibitor in the tumor microenvironment compared to adjacent healthy tissue [33]. On the other hand, the COX-2 positive A2058 xenograft model shows higher signal intensity as well as a better signal-to-noise ratio in the tumor tissue 5 h post injection. However, both xenotransplanted animal models show compound enrichment in subcutaneous fat, which is complicating the differentiation between specific fluorescence signal and unspecific subcutaneous signal within the whole animal acquisitions obtained from nude NMRI mice. Nevertheless, cryosections clearly reveal enrichment of the inhibitor in the COX-2 expressing A2058 tumors but not in the COX-2 negative A375 tumors. According to the higher COX-1 protein level of A375-pIRES tumor xenograft we confirmed that no unselective binding of **C1** to the structurally similar COX-1 isoenzyme occurs confirming former results [16,22,23]. The cryosections of the COX-2-negative A375 tumor bearing mice show a higher unspecific enrichment in adipose tissue compared to the A2058 tumor bearing animals. Although the substance is very lipophilic (logP(**C1**) = 4.39, calculated with ALOGPS) there is only a low unspecific enrichment in adipose tissue in the A2058 tumor bearing mice. Taken together, using an autofluorescent COX-2 inhibitor visualization of TPA-induced and human melanoma xenografts *in vivo* and *ex vivo* was allowed and differentiation between COX-2-expressing and COX-2-negative tumor xenotransplants was clearly possible. On the other hand, the whole animal acquisitions revealed problems associated with the biodistribution of **C1** because the compound showed substantial enrichment in the subcutaneous fat. Due to the specific wavelengths ($\lambda_{Ex.} = 345$ nm, $\lambda_{Em.} = 482$ nm) that have to be used for the autofluorescent inhibitor, tissue penetration is severely limited. Therefore, the whole animal acquisition only gives a superficial two-dimensional distribution of the compound with less than

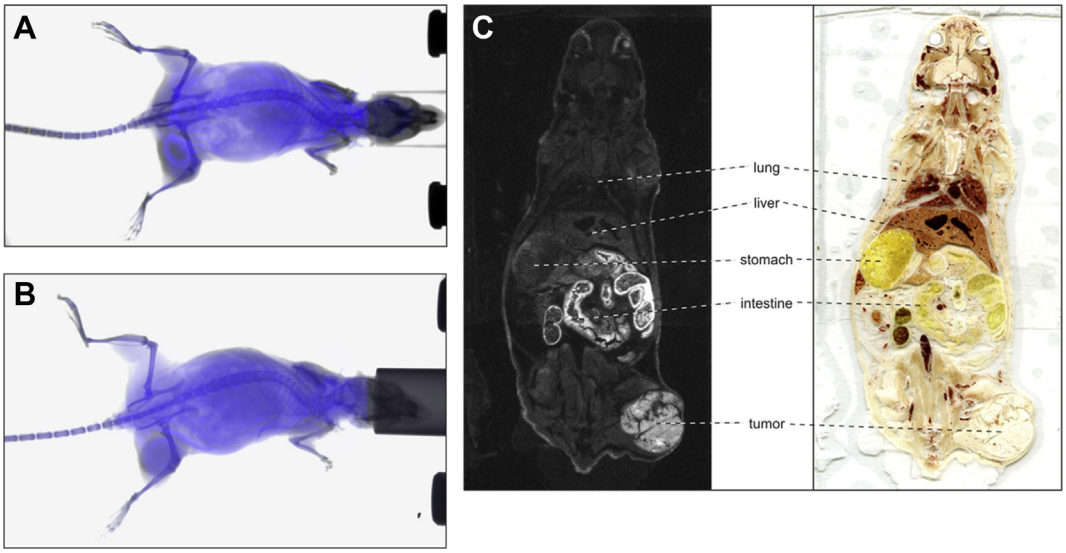

Fig. 4. A2058 tumor xenograft model Whole animal acquisition of A2058 tumor bearing mice at (A) 5 h and (B) 24 h after i.p. injection of 100 μL 20 mM **C1**, exposure time 15 min, binning 4 × 4; (C) cryosection 24 h after i.p. injection of **C1**, exposure time 30 min. The figure shows representative images out of 5 independent experiments.

1 mm penetration depth. In contrast, fluorophores with longer excitation and emission wavelengths like near infrared and infrared dyes show higher tissue penetration up to several millimeters [21,30,31]. On the other hand investigations by Tanaka et al. [34] using three different ^{11}C-labeled diaryl-substituted imidazole or indole derivatives as PET-agents which allow for high tissues penetration and have lower lipophilicity ($\log P_{7.4} = 1.9–2.3$) showed no specific enrichment in COX-2 expressing AH109A tumors after 60 min. Therefore, the use of fluorescence COX-2 inhibitors revealed advantages regarding the time window for observation (24 h and longer). Taken together, *ex vivo* cryosections demonstrated a high specificity of **C1** to COX-2. In addition, we were able to examine pharmacological properties of this autofluorescent COX-2 inhibitor (without an additional fluorophore) as a representative of a novel indole-based group of coxibs. Despite the fact that animals can tolerate small amounts of DMSO [35] application in DMSO is not transferable to medical practice in humans. Nevertheless, we present new data about the general distribution and hepatobiliary elimination properties of this COX-2 inhibitor. Compared to previous work of other groups [21,36] the herein presented indole-based COX-2 inhibitor offers distinct advantages due to its autofluorescent properties, which eliminates the need for additional fluorophore or radiolabeling of the coxib. Therefore, no sterically demanding group, which might lower the inhibitory efficacy or change the pharmacological properties of the coxib had to be introduced. Because of the selective binding of the inhibitor to COX-2 expressing tissues *in vivo* and its autofluorescent properties [16], the compound **C1** is a potential substance to combine therapeutic approaches, *in situ* guided surgery, and *ex vivo* diagnostics and makes it interesting as well as promising for further effect studies, e.g., antioxidant, radioprotective, and radiosensitizing activities [37,38].

Conflict of interest

The authors declare no conflict of interest.

Acknowledgments

The excellent technical assistance of Catharina Heinig, Mareike Barth and Aline Morgenegg is greatly acknowledged. The authors are grateful to Ralf Bergmann, Ph.D., for his expert advice in animal experiments and many fruitful discussions. The authors thank the Helmholtz Association for funding of this work through Helmholtz-Portfolio Topic “Technologie und Medizin – Multimodale Bildgebung zur Aufklärung des In-vivo-Verhaltens von polymeren Biomaterialien”. This work is part of the research initiative Radiation-Induced Vascular Dysfunction (RIVAD) Research Network. Sandra Ullm is recipient of a fellowship by Europäische Sozialfonds (ESF).

Transparency document

The transparency document associated with this article can be found in the online version at http://dx.doi.org/10.1016/j.bbrc.2015.01.057.

References

[1] D.L. Simmons, R.M. Botting, T. Hla, Cyclooxygenase isozymes: the biology of prostaglandin synthesis and inhibition, Pharmacol. Rev. 56 (2004) 387–437.
[2] B.B. Aggarwal, P. Gehlot, Inflammation and cancer: how friendly is the relationship for cancer patients? Curr. Opin. Pharmacol. 9 (2009) 351–369.
[3] J.J. Lee, M. Natsuizaka, S. Ohashi, G.S. Wong, M. Takaoka, C.Z. Michaylira, D. Budo, J.W. Tobias, M. Kanai, Y. Shirakawa, Y. Naomoto, A.J. Klein-Szanto, V.H. Haase, H. Nakagawa, Hypoxia activates the cyclooxygenase-2-prostaglandin E synthase axis, Carcinogenesis 31 (2010) 427–434.
[4] G. Daneau, R. Boidot, P. Martinive, O. Feron, Identification of cyclooxygenase-2 as a major actor of the transcriptomic adaption of endothelial and tumor cells to cyclic hypoxia: effect on angiogenesis and metastases, Clin. Cancer Res. 16 (2010) 410–419.
[5] T. Kniess, M. Laube, R. Bergmann, F. Sehn, F. Graf, J. Steinbach, F. Wuest, J. Pietzsch, Radiosynthesis of a ^{18}F-labeled 2,3-diarylsubstituted indole via McMurry coupling for functional characterization of cyclooxygenase-2 (COX-2) *in vitro* and *in vivo*, Bioorg. Med. Chem. 20 (2012) 3410–3421.
[6] G.F. Benderro, J.C. LaManna, HIF-1α/COX-2 expression and mouse brain capillary remodeling during prolonged moderate hypoxia and subsequent re-oxygenation, Brain Res. 1569 (2014) 41–47.
[7] H.R. Roberts, H.J. Smartt, A. Greenhough, A.E. Moore, A.C. Williams, C. Paraskeva, Colon tumour cells increase PGE(2) by regulating COX-2 and 15-PDGH to promote survival during the microenviromental stress of glucose deprivation, Carcinogenesis 32 (2011) 1741–1747.
[8] K. Gupta, G.J. Fisher, J.T. Elder, J.J. Voorhees, Sphingosin inhibits phorbol ester-induced inflammation, ornithine decarboxylase activity, and activation of protein kinase C in mouse skin, J. Invest. Dermatol. 91 (1988) 486–491.
[9] H.Q. Wang, R.C. Smart, Overexpression of protein kinase C-alpha in the epidermis of transgenic mice results in striking alterations in phorbol ester-induced inflammation and COX-2, MIP-2 and TNF-alpha expression but not tumor promotion, J. Cell. Sci. 112 (1999) 3497–3506.
[10] Y.-J. Jung, J.S. Isaacs, S. Lee, J. Trepel, L. Neckers, IL-1β-mediated up-regulation via an NFκB/COX-2 pathway identifies HIF-1 as a critical link between inflammation and oncogenesis, FASEB J. 17 (2003) 2115–2117.
[11] K. Sommer, B. Guo, J.L. Pomerantz, A.D. Bandaranayake, M.E. Moreno-García, Y.L. Ovechkina, D.J. Rawlings, Phosphorylation of the CARMA1 linker controls NF-kappB activation, Immunity 23 (2005) 561–574.
[12] D. Wang, R.N. DuBois, Eicosanoids and cancer, Nat. Rev. 10 (2010) 181–193.
[13] C. Denkert, M. Köbel, S. Berger, A. Siegert, A. Leclere, U. Trefzer, S. Hauptmann, Expression of cyclooxygenase 2 in human malignant melanoma, Cancer Res. 61 (2001) 303–308.
[14] T.W. Davis, J.M. O'Neal, M.D. Pagel, B.S. Zweifel, P.P. Mehta, D.M. Heuvelman, J.L. Masferrer, Synergy between celecoxib and radiotherapy results from inhibition of cyclooxygenase-2-derived prostaglandin E 2, a survival factor for tumor and associated vasculature, Cancer Res. 64 (2004) 279–285.
[15] L.J. Marnett, The COXIB experience: a look in the rearview mirror, Annu. Rev. Pharmacol. Toxicol. 49 (1) (2009) 265–290.
[16] M. Laube, C. Tondera, S.K. Sharma, N. Bechmann, F.-J. Pietzsch, A. Pigorsch, M. Köckerling, F. Wuest, J. Pietzsch, T. Kniess, 2,3-diaryl-substituted indole based COX-2 inhibitors as leads for imaging tracer development, RSC Adv. 4 (2014) 38726–38742.
[17] J.R. Lakowicz, S. Keating, Binding of an indole derivative to micelles as quantified by phase-sensitive detection of fluorescence, J. Biol. Chem. 258 (1983) 5519–5524.
[18] D. Bonne, C. Heuséle, C. Simon, D. Pantaloni, 4′,6-diamidino-2-phenylindole, a fluorescent probe for tubulin and microtubules, J. Biol. Chem. 260 (1985) 2819–2825.
[19] A. Bhardwaj, J. Kaur, S.K. Sharma, Z. Huang, F. Wuest, E.E. Knaus, Hybrid fluorescent conjugates of COX-2 inhibitors: search for a COX-2 isozyme imaging cancer biomarker, Bioorg. Med. Chem. Lett. 23 (2013) 163–168.
[20] A. Bhardwaj, J. Kaur, F. Wuest, E.E. Knaus, Fluorophore-labeled cyclooxygenase-2 inhibitors for the imaging of cyclooxygenase-2 overexpression in cancer: synthesis and biological studies, ChemMedChem 9 (2014) 109–116.
[21] J. Uddin, B.C. Crews, A.L. Blobaum, P.J. Kingsley, D.L. Gorden, J.O. McIntyre, L.M. Matrisian, K. Subbaramaiah, A.J. Dannenberg, D.W. Piston, L.J. Marnett, Selective visualization of cyclooxygenase-2 in inflammation and cancer by targeted fluorescent imaging agents, Cancer Res. 70 (2010) 3618–3627.
[22] W. Hu, Z. Guo, F. Chu, A. Bai, X. Yi, G. Cheng, J. Li, Synthesis and biological evaluation of substituted 2-sulfonyl-phenyl-3-phenyl-indoles: a new series of selective COX-2 inhibitors, Bioorg. Med. Chem. 11 (2003) 1153–1160.
[23] C. Tondera, M. Laube, C. Wimmer, T. Kniess, B. Mosch, K. Großmann, J. Pietzsch, Visualization of cyclooxygenase-2 using a 2,3-diarylsubstituted indole-based inhibitor and confocal laser induced cryofluorescence microscopy at 20 K in melanoma cells *in vitro*, Biochem. Biophys. Res. Commun. 430 (2013) 301–306.
[24] Imada, E.F. Sato, M. Miyamoto, Y. Ichimori, Y. Minamiyama, R. Konaka, M. Inoue, Analysis of reactive oxygen species generated by neutrophils using a chemiluminescence probe L-012, Anal. Biochem. 271 (1999) 53–58.
[25] Kielland, T. Blom, K.S. Nandakumar, R. Holmdahl, R. Blomhoff, H. Carlsen, In vivo imaging of reactive oxygen and nitrogen species in inflammation using the luminescent probe L-012, Free Radic. Biol. Med. 47 (2009) 760–766.
[26] Zhou, Y.-T. Tsai, H. Weng, L. Tang, Noninvasive assessment of localized inflammatory responses, Free Radic. Biol. Med. 52 (2012) 218–226.
[27] Mosch, D. Pietzsch, J. Pietzsch, Irradiation affects cellular properties and Eph receptor expression in human melanoma cells, Cell. Adh. Migr. 6 (2012) 113–125.
[28] Mamat, B. Mosch, C. Neuber, M. Knöckerling, R. Bergmann, J. Pietzsch, fluorine-18 radiolabeling and radiopharmacological characterization of a benzodioxolylpyrimidine-based radiotracer targeting the receptor tyrosine kinase EphB4, ChemMedChem 7 (2012) 1991–2003.
[29] S. Ullm, A. Krüger, C. Tondera, T.P. Gebauer, A.T. Neffe, A. Lendlein, F. Jung, J. Pietzsch, Biocompatibility and inflammatory response in vitro and in vivo to gelatin-based biomaterials with tailorable elastic properties, Biomaterials 35 (2014) 9755–9766.

[30] Shah, R. Weissleder, Molecular optical imaging: applications leading to the development of present day therapeutics, NeuroRX 2 (2005) 215–225.
[31] D.M. Olive, Near Infrared Technology and Optical Agents for Molecular Imaging, Application Note, LI-COR Biosciences, Licoln, USA, 2006.
[32] D. Tracey, L. Klareskog, E.H. Sasso, J.G. Salfeld, P.P. Tak, Tumor necrosis antagonist mechanisms of action: a comprehensive review, Pharmacol. Ther. 117 (2008) 244–279.
[33] H. Maeda, J. Wu, T. Sawa, Y. Matsumura, K. Hori, Tumor vascular permeability and the EPR effect in macromelecular therapeutics: a review, J. Control. Release 65 (2000) 271–284.
[34] M. Tanaka, Y. Fujisaki, K. Kawamura, K. Ishiwatat, Quinggeletu, F. Yamamoto, T. Mukai, M. Maeda, Radiosynthesis and evaluation of ^{11}C-labeled diaryl-substituted imidazole and indole derivatives for mapping cyclooxygenase-2, Biol. Pharm. Bull. 29 (2006) 2087–2094.
[35] P. Montaguti, E. Melloni, E. Cavaletti, Acute intravenous toxicity of dimethyl sulfoxide, polyethylene glycol 400, dimethylformamide, absolute ethanol, and benzyl acohol in inbred mouse strains, Drug Res. 44 (1994) 566–570.
[36] S.L. Timofeevski, J.J. Prisakiewicz, C.A. Rouzer, L.J. Marnett, Isoform-selective interaction of cyclooxygenase-2 with indomethacin amides studied by real-time fluorescence, inhibition kinetics, and site-directed mutagenesis, Biochemistry 41 (2002) 9654–9662.
[37] J. Pietzsch, M. Laube, N. Bechmann, F. Pietzsch, T. Kniess, Protective effects of 2,3-diaryl-substituted indole-based cyclooxygenase-2 inhibitors on oxidative modification of human low density lipoproteins in vitro, Clin. Hemorheol. Microcirc. (2014 Dec 29) [Epub ahead of print] PMID: 25547413.
[38] S. Ullm, M. Laube, N. Bechmann, T. Kniess, J. Pietzsch, Organotypical vascular model for characterization of radioprotective compounds: studies on anti-oxidant 2,3-diaryl-substituted indole-based cyclooxygenase-2 inhibitors, Clin. Hemorheol. Microcirc. 58 (2014) 281–295.